INTERFACE

rsif.royalsocietypublishing.org

Research

Cite this article: David S, Funken J, Potthast W, Blanke A. 2016 Musculoskeletal modelling under an evolutionary perspective: deciphering the role of single muscle regions in closely related insects. *J. R. Soc. Interface* **13**: 20160675.
http://dx.doi.org/10.1098/rsif.2016.0675

Received: 23 August 2016
Accepted: 7 September 2016

Subject Category:
Life Sciences–Engineering interface

Subject Areas:
evolution, biomechanics

Keywords:
musculoskeletal modelling, bite force, dragonfly, insect, mouthparts, functional constraints

Author for correspondence:
Alexander Blanke
e-mail: a.blanke@hull.ac.uk

†These authors contributed equally to this study.

Electronic supplementary material is available online at https://dx.doi.org/10.6084/m9.figshare.c.3473643.

THE ROYAL SOCIETY PUBLISHING

Musculoskeletal modelling under an evolutionary perspective: deciphering the role of single muscle regions in closely related insects

Sina David[1,†], Johannes Funken[1], Wolfgang Potthast[1,2] and Alexander Blanke[3,†]

[1]Institute of Biomechanics and Orthopaedics, German Sport University Cologne, Cologne 50933, Germany
[2]ARCUS Clinics Pforzheim, Rastatter Strasse 17-19, 75179 Pforzheim, Germany
[3]Medical and Biological Engineering Research Group, School of Engineering, University of Hull, Hull HU6 7RX, UK

AB, 0000-0003-4385-6039

Insects show a remarkable diversity of muscle configurations, yet the factors leading to this functional diversity are poorly understood. Here, we use musculoskeletal modelling to understand the spatio-temporal activity of an insect muscle in several dragonfly species and to reveal potential mechanical factors leading to a particular muscle configuration. Bite characteristics potentially show systematic signal, but absolute bite force is not correlated with size. Muscle configuration and inverse dynamics show that the wider relative area of muscle attachment and the higher activity of subapical muscle groups are responsible for this high bite force. This wider attachment area is, however, not an evolutionary trend within dragonflies. Our inverse dynamic data, furthermore, show that maximum bite forces most probably do not reflect maximal muscle force production capability in all studied species. The thin head capsule and the attachment areas of muscles most probably limit the maximum force output of the mandibular muscles.

1. Background

Insect outer anatomy is extremely diverse [1] and reflected by the diversity of their inner anatomy [2,3]. Apart from many other anatomical details, muscle arrangements, muscle size and muscle presence are subject to high variation across the insect orders [2,4–6], but notably also within family representatives [7].

Muscle arrangements and their absence and presence in insect lineages are frequently coded as morphological characters subsequently used in systematics [5,6,8]. Identifying factors that influence muscle equipment could aid our understanding of the causes of muscle evolution within and across lineages. Given the vast morphological diversity of insects, model systems are needed to indentify key factors governing muscle configuration, while other factors, such as ecology or embryological development, remain stable and thus do not have to be taken into account. Dragonflies (Odonata) are such a model system. They are predators with an overall similar gross cephalic morphology and similar ecological niches [9]. For example, all dragonflies are predators of other insects, which means that their mouthparts handle the same overall food spectrum [9]. Thus, it is possible to investigate the influence of variations within the mandibular muscles in multiple species, disregarding ecological factors such as food spectrum or largely differing head and mandibular geometries (as would be present between, for example, grasshoppers and beetles). Additionally, their bite force is comparably easy to measure due to their large mouthparts and gape angles [10]. In all dragonfly species, the mandibles are connected to the head with two ball-and-socket joints each; the muscle equipment consists of a large single mandibular adductor, an abductor and a varying set of three or four smaller associated adductors [8,11–13]. It has been shown [10]

that these additional adductors use approximately 15% of their potential activity during biting and that they have a negligible effect during biting. Descriptive studies have shown that the volumes and muscle arrangements of these muscles do not change among dragonflies [7,14]. By contrast, the muscle geometry of the main mandibular adductor is variable among dragonflies, ranging from comparably simple geometries with a uniform attachment area at the inner backside of the head to muscles with clearly defined subgroups in a more medial position (henceforth, subapical muscle groups). Studies of muscle architecture in humans have shown that factors such as a shorter muscle fibre length and greater cross-sectional area have an impact on force generation [15–17]. In insects, variation of the main mandibular adductor muscle is even higher among other chewing–biting insect orders such as stoneflies, grasshoppers, beetles or bees [18]. It is speculated that these different muscle configurations are related to the respective food spectrum and the head capsule form of the particular insect [3,18]. However, this does not explain variation within, for example, dragonflies, as head morphology at the backside of the head is the same, as is mandibular morphology and food spectrum.

We expect these subapical muscle groups, which are present only in some dragonflies, to show unusually high activity levels compared with the rest of the muscle as this would explain their presence and perhaps point towards phylogenetic signal. We also expect dragonflies which show these subapical muscle subgroups to have a mechanically more advantageous mandibular muscle lever setting, i.e. they are able to transmit more of the muscle force to the food item. The wider attachment area will also lead to higher absolute bite forces.

In order to evaluate these theories, we carried out musculoskeletal modelling, a simulation approach which has been proved to be useful to address a diverse range of questions related to human [19] and animal movement [20–22], including biting [23–27]. Given precise geometrical and physiological input data, it is possible to simulate the spatio-temporal activity and force levels of muscles and even subparts of muscles [25,28–30]. This gives an indication of the overall influence of a muscle on a dynamic system and thus allows the functional importance of a given muscle to be assessed. By using musculoskeletal modelling in a comparative approach it might indicate the evolutionary significance of specific muscle configurations when compared between a range of species.

2. Material and methods

2.1. Bite force measurements

Living *Aeshna cyanea*, *Anax imperator* (Anisoptera: Aeshnidae), *Cordulegaster bidentata* (Anisoptera: Cordulegastridae), *Onychogomphus forcipatus* (Anisoptera: Gomphidae) and *Sympetrum vulgatum* (Anisoptera: Libellulidae) specimens were used for our experiments. For the sake of brevity, only genus names will be used in the following. Bite force measurements (figure 1*a*) were carried out with a 0.60 mm thick mini force sensor (SKB piezoelectric pin-force sensor Z18152X2A3sp; Kistler, Winterthur, Switzerland). Bite forces of *Cordulegaster* were captured using a sensor of 0.80 mm thickness (SKB pin-force sensor Z18152X2A7sp; Kistler). Dragonflies were fixed at the thorax with a custom-built fixation device (figure 1*a*), the sensor was moved between the mouthparts and bites were recorded for 30–150 s, depending on the dragonflies' biting behaviour. Bite signal was filtered (Butterworth, low pass, 4th order, 50 Hz cut-off, recursive) and used as the input for the respective mandibular muscle model. The 10 strongest bites out of one bite cycle series for

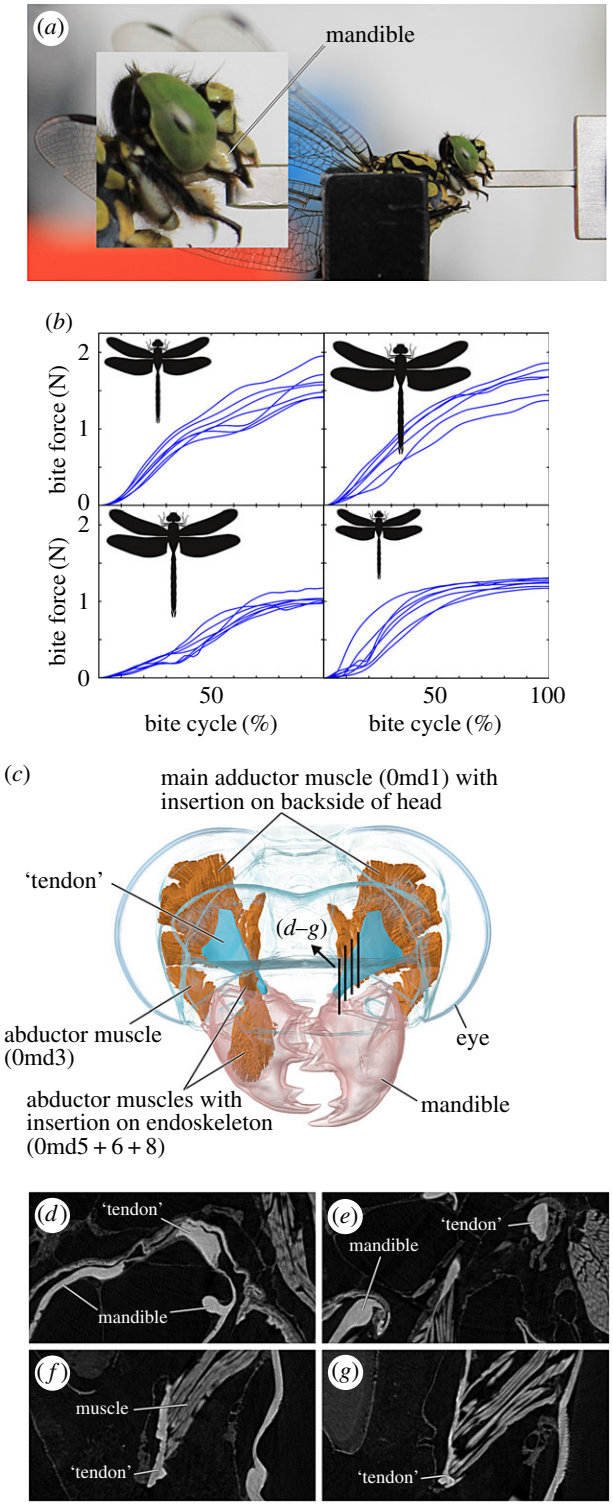

Figure 1. Experimental set-up and bite force time series. (*a*) Lateral view of the dragonfly *Onychogomphus forcipatus* biting onto the piezoelectric force sensor. (*b*) Bite time series showing the progression of bite force until the peak bite force is reached. From left to right: *Aeshna mixta*, *Anax imperator*, *Cordulegaster bidentata*, *Onychogmphus forcipatus*. Line drawing representations of dragonflies are in proportion to each other. Note the comparably high bite force of *O. forcipatus* compared with its body size. (*c*) Three-dimensional model of the head of *O. forcipatus* in frontal view showing the mandibular muscle configuration. Abbreviations: 0md1, M. craniomandibularis internus; 0md3, M. craniomandibularis externus posterior; 0md5, M. tentoriomandibularis lateralis superior; 0md6, M. tentoriomandibularis lateralis inferior; 0md8, M. tentoriomandibularis medialis inferior. (*d–g*) Sagittal cross sections through the tendon–muscle connection to show the similarity in grey values between the 'tendon' and the mandible. Refer to (*c*) for the location of the cross sections. The same grey values relate to the same material density, which can relate to material properties.

Table 1. Overview of the bite forces, bite times and muscle parameters measured. Bite frequencies were extracted from the full dataset of bite force measurements, other values are based on the 10 strongest bites recorded. 0md1, M. craniomandibularis internus. *F*, force; MA, mechanical advantage.

species	*Anax imperator*	*Aeshna mixta*	*Onychogomphus forcipatus*	*Cordulegaster bidentata*	*Sympetrum vulgatum*[a]
F_{mean} (N)	1.62 ± 0.20	1.53 ± 0.19	1.23 ± 0.05	1.02 ± 0.06	0.24 ± 0.03
F_{max} (N)	1.91	1.95	1.31	1.17	0.31
bite duration (ms)	166.8 ± 30.9	135.2 ± 21.8	458.1 ± 187.8	367.1 ± 36.0	197.5 ± 51.3
bite freq. (Hz)	4.5	5.0	2.0	1.5	3.5
time to max. *F* (ms)	92 ± 25.2	71.6 ± 13.3	209.8 ± 60.3	218.8 ± 45.7	95.8 ± 27.3
time to max. *F* (% Bite)	54.2 ± 6.3	52.5 ± 2.5	50.6 ± 16.9	59.1 ± 6.6	52.3 ± 3.7
0md1 attachment area (mm^2)	4.44	4.95	3.51	5.03	1.44
size corrected attachment area	0.42	0.62	0.54	0.50	0.25
muscle stress ($N\,cm^{-2}$)	43.0	39.4	37.3	23.3	21.5
MA	0.38	0.41	0.40	0.39	0.41

[a]Species studied previously [10]; values are presented here for comparison.

each dragonfly were extracted and used for calculation of the discrete force parameters presented in table 1. In the following, only seven out of these 10 bites were analysed with respect to muscle activation patterns (five strongest, one medium and the weakest bite). The complete bite recordings are available as electronic supplementary material, figure S1.

2.2. Kinematic muscle model set-up

High-resolution synchrotron radiation micro-computed tomography (SR-μCT) was carried out to derive the detailed inner anatomies for the investigated species. The SR-μCT set-up and preparation followed our earlier studies on insects [7,12,14] and established protocols of the respective beamlines used [31,32].

2.3. Creation of a musculoskeletal model

Model creation followed the procedures explained in detail in our earlier study [10]; therefore, only the most crucial steps are mentioned in the following. SR-μCT data were segmented with ITK-snap [33] and three-dimensional models were exported as stl-files into Blender (figure 1*c*; v2.77, www.blender.org) for smoothing and alignment to each other. All models were normalized for size with respect to the *Sympetrum* set-up of the earlier study [10] in order to allow for direct comparison of the spatio-temporal activity levels. Muscle representations were then exported in obj-format into the AnyBody™ modelling system; all rigid segments, such as tendons, were exported as stl-files. All rigid segments were attached to their respective centre of mass. The models contain two joints at the mandible as this is the *in vivo* morphology for dragonflies. This leads to a virtual revolute joint, which eliminates five of the six theoretical degrees of freedom. The range of motion of the virtual revolute joints was extracted from the video footage of the biting sequences. The origin and insertion points of the muscles were connected with 'viapoint' muscles in AnyBody, which means that the muscle length is simulated as the shortest distance between the origin and insertion point of a given muscle in a non-static condition. This is in agreement with the geometric muscle relations based on morphological data of dragonflies (figures 1*c* and 2*a*) [7,14]. Tendon geometry was modelled according to the *in vivo* morphology. Although termed 'tendon', these structures in insects are partly heavily sclerotized [34,35] and our μCT data corroborate these findings for dragonflies (figure 1*d–g*). Owing to this sclerotization, the material properties of this structure most probably cannot be compared with tendon-like structures in, for example, vertebrates (see Discussion). Previous analyses in vertebrates showed that tendons are very stiff in material behaviour [36], thus we modelled the large 'tendon' of M. craniomandibularis internus as a rigid segment. In order to ensure a natural movement of the 'tendon' a new insertion point (M1) at the head capsule was created, which is the midpoint of all head capsule insertions. From this point, a viapoint muscle between M1 and the 'tendon' insertion at the mandible (M2) was created. The geometric centre of the 'tendon' was then defined to be the midpoint between M1 and M2. Kinematic simulations were carried out to record the tendon movement; the resultant vector was transferred into a .c3d file. This motion file was used as a marker to lead the tendon movement after implementing all the muscle fibres of the main adductor muscle. The muscle insertions at the 'tendon' and the insertion of the 'tendon' at the mandible were then converted into the tendons' coordinate system with the origin described above.

2.4. Muscle model

All muscles were modelled with the 'SimpleMuscle' Hill-type model provided by the AnyBody system. This ignores the differing behaviour of contractile and non-contractile elements in a given muscle fibre and requires only the definition of the initial muscle force. As previous studies found good agreement between the 'SimpleMuscle' model and more parameter intensive models when slower movements are simulated [28,37], and due to the fact that characteristics such as initial muscle force, contraction velocity and length of the non-contractile elements are unknown for dragonfly head muscles, the usage of the 'SimpleMuscle' model is currently the best working hypothesis [38]. Additionally, all muscle regions within the mandibular muscles were modelled as equally strong. Previous studies investigating muscle property variation in a range of ants reported larger differences in muscle architecture if species show a different food spectrum and differing ecological niches [34,35]. The same studies also reported an overall similarity of muscle characteristics if the ecological niche is similar. Dragonflies show the same larval development and the same food preferences. Although copulatory behaviour varies, dragonflies do not use their mouthparts before or during copulation (like, for example, stag beetles [39–41] or tiger beetles [42]). Owing to the high similarities in all factors previously reported as responsible for changing mandibular muscle architecture, we believe that our approach of modelling each muscle region as equally strong is justified.

For our simulations, we assumed that the dragonflies bite with their respective maximum bite force. During the measurements we used a cushioned calliper-like fixation to press

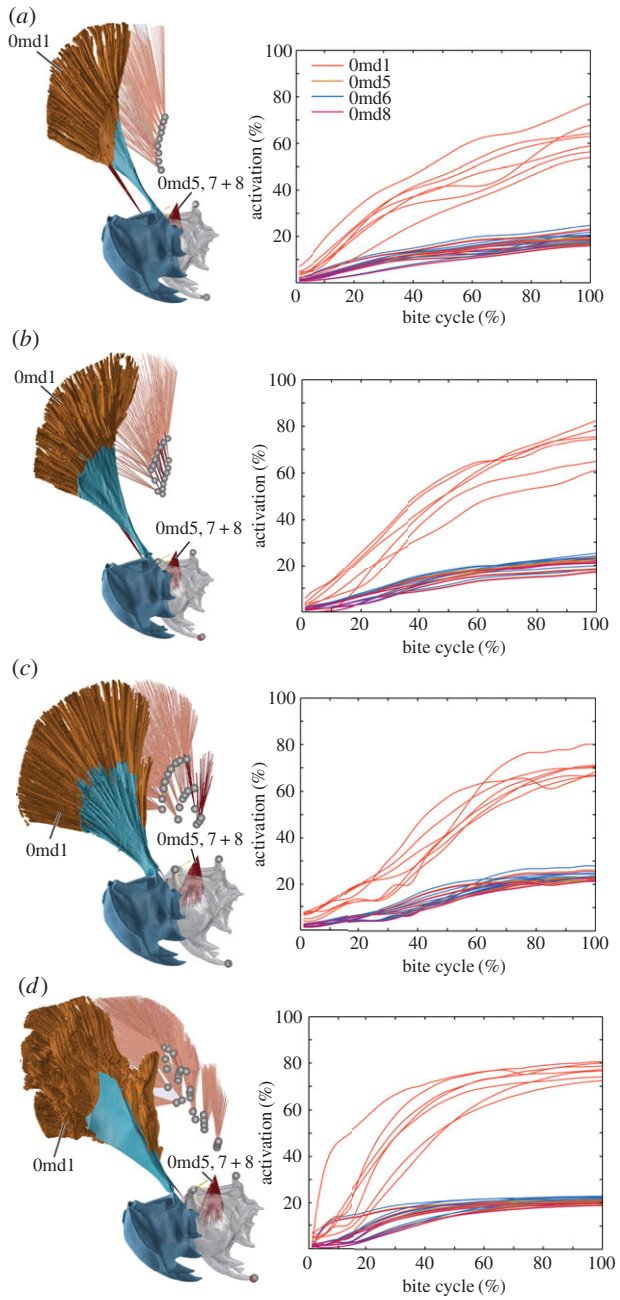

Figure 2. Overview of muscle geometry (left) and muscle activation (right) in the investigated species *Aeshna/Sympetrum* set-up (*a*), *Anax imperator* (*b*), *Cordulegaster bidentata* (*c*) and *Onychogomphus forcipatus* (*d*). Segmented three-dimensional models are shown in front of AnyBody inverse dynamic models. Both models are of the right side of the head; slight differences in perspective are due to the different programs used for the respective model (Blender/AnyBody). All models are corrected for size; 'tendon' is in light blue, mandible in dark blue or grey, respectively. 'Tendon' is omitted in the AnyBody models to better show different muscle groups. Time series show activation for each mandibular muscle during the 10 strongest bites measured. Activation was normalized against the maximum force modelled for each fibre; bite cycle duration was normalized against contact time. Abbreviations: 0md1, M. craniomandibularis internus; 0md5, M. tentoriomandibularis lateralis superior; 0md6, M. tentoriomandibularis lateralis inferior; 0md8, M. tentoriomandibularis medialis inferior.

repeatedly against the thorax of the specimens as this represents a strong neuronal input.

Regarding the muscle recruitment criterion of our musculoskeletal modelling approach, we are in line with other studies in that we used a quadratic muscle recruitment criterion that optimizes fibre recruitment by evenly distributing activation across all involved fibres according to their location within the muscle. Methods testing the accuracy of numerical models concluded that minimization of squared or cubed muscle stresses most closely reflected experimental data [43–46], while Rasmussen *et al*. [45] pointed out that cubed optimization criteria create numerical difficulties. Musculoskeletal models with multiple muscle strands per single muscle have been reported as beneficial with regard to model accuracy [27]. We modelled the muscles with very high strand quantities (table 1) to derive more accurate data of the spatio-temporal activity.

2.5. Simulation set-ups for spatial muscle composition

The mandibular muscle system of the investigated species is mainly composed of five muscles, one abductor (M. craniomandibularis externus posterior; 0md3) and four adductors ((figure 1*c*; M. craniomandibularis internus, 0md1; M. tentoriomandibularis lateralis superior, 0md5; M. tentoriomandibularis lateralis inferior, 0md6; M. tentoriomandibularis medialis inferior, 0md8) which are responsible for movement of the mandible: 0md1+3 originate at the head capsule; 0md5+6+8 (henceforth 0md5–8) originate at the tentorium—an X-shaped chitinous structure within the head of insects which connects each arm to the head capsule.

Previous studies have demonstrated that the very small muscles 0md5–8 show low activity levels during biting. These muscles are highly similar across dragonfly species concerning geometry, origin and insertion [7,11]. Therefore, we focused on a detailed investigation of the largest muscle in the dragonfly head, M. craniomandibularis internus (0md1). The muscle partitioning scheme for 0md1 is artificial as it is focused on a comparison of muscle groups at certain locations between species. This was done as follows: the *Aeshna/Sympetrum* muscle set-up is the simplest setting with nine groups (G1–9) attaching at the end of the main adductor 'tendon'. We modelled this setting by changing muscle origins and tendon insertions according to the µCT data for *Aeshna* but disregarding tendon nearer to the mandible insertion of the 'tendon' (figure 2*a*). This ensures that we can compare the slightly differing geometry of the main mandibular muscle of *Aeshna* and *Anax* with an earlier study of the mandibular muscles of the dragonfly *Sympetrum vulgatum* [10], where these nine muscle groups were also simulated. The *in vivo* muscle configuration in the closely related species *Aeshna* and *Anax* is similar. By modelling the main adductor muscle with and without the medial muscle subgroups (*Aeshna/Sympetrum* versus *Anax/Aeshna* configuration), we were able to investigate the influence of these additional muscle groups on overall muscle activity. The main mandibular muscle of *Anax/Aeshna* was additionally modelled with seven subgroups nearer to the mandible insertion of the 'tendon' (G10–16, figure 2*b*) in addition to the nine lateral (main) muscle groups from the *Aeshna/Sympetrum* set-up (G1–9). *Cordulegaster* shows an even higher complexity with two distinguishable medial muscle subgroups (G1 – 3 + 5 and G4 + 6 – 10; figure 2*c*); again, the number of the main muscle groups was kept the same (G12–19). Finally, *Onychogomphus* shows the main mandible adductor with the highest grade of complexity so far observed in dragonflies [7,14] with a whole cascade of medial muscle subgroups (figure 2*d*).

2.6. Further measurements

Apart from the bite force measurements, we calculated the mandibular mechanical advantage (MA) for each species based on lever arm measurements. As the dicondylous insect mandible is a third-order lever just like in vertebrates [47,48], the MA is the ratio between the inner lever arm and the outer lever arm. The MA indicates the relative force transmissions of the muscle force to the food item, which is correlated with diet in, for example, vertebrates and thus is a frequently used proxy to assess the biomechanical disparity of the mandibular muscle insertions and joints among taxa [49,50]. Physiological

Table 2. Correlations of muscle and 'tendon' modelling parameters with muscle activity. MT, muscle–tendon; ORTH, orthogonal to the tendon plane; PLANE, in line with the tendon plane; MT ratio, muscle–tendon length ratio. First value, *p*-value; correlation coefficient (*R*) in brackets.

species	activation–MT angle ORTH	activation–MT angle PLANE	activation–MT ratio
Anax imperator	0.180 (−0.38)	0.265 (−0.21)	0.612 (0.16)
Aeshna mixta	0.824 (−0.05)	0.119 (0.44)	0.505 (−0.13)
Onychogomphus forcipatus	0.726 (0.05)	0.02 (−0.31)	0.793 (0.19)
Cordulegaster bidentata	0.580 (−0.09)	0.092 (−0.28)	0.308 (0.04)
Sympetrum vulgatum[a]	0.476 (−0.22)	0.612 (0.16)	0.358 (−0.27)

[a]Again, values for *Sympetrum* based on [10] are presented for direct comparison with the specimens studied here.

cross-sectional areas (PCSAs) were measured in the µCT data at the attachment sites of the respective muscles.

Our modelling is an inevitable simplification, especially with regards to 'tendon' simulation and the quantity of muscle fibres (see Discussion). To test whether the observed activation patterns where dependent on the way we modelled the muscles and 'tendons', we measured 'tendon' length and muscle length and calculated the tendon–muscle length ratio for each muscle group and correlated this ratio with activation levels at the peak of the strongest bite using Kendall's τ coefficient. This gave us an indication of whether muscle activations are dependent on our simplifying assumption that the 'tendon' is a stiff structure, as tendon–muscle length ratios vary depending on the muscle group.

Furthermore, we measured the insertion angle for each muscle group to test (again with Kendall's τ coefficient) whether muscle activity was dependent on the angle of insertion on the 'tendon'. For this we did two measurements: one in the plane of the 'tendon', the other one orthogonal to it.

3. Results

3.1. Bite force

In total, 1934 bites were recorded (electronic supplementary material, figure S1). Peak bite forces ranged from 0.31 to 1.95 N; larger species with larger PCSAs showed higher bite forces (table 1). An exception is *Cordulegaster*, which showed a bite force around 1 N, although it is the largest species also with respect to PCSA. Taking into account measured PCSAs and mandibular lever arms, muscle stress is species dependent in the range of 21.5–43N cm^{-2}. Bite duration ranged from 135 to 458 ms; all species, except *Cordulegaster* (60%), reached their peak force at around 50% of the bite (table 1).

3.2. General muscle activation levels

Correlations of activation with the muscle–tendon length ratio and our other measured values in each species were not significant (table 2), except for a correlation of the muscle insertion angle in *Onychogomphus*. The large mandibular adductor shows the highest activation in each species (figure 2). Associated smaller intramandibular muscles 0md5–8 generally ranged around 20% activity. Time series of muscle activation are closely related to the bite time series (figure 1*b* and 2), and these are distinctly different in the species studied. Aeshnidae (*Anax* + *Aeshna*) shows an approximately linear increase in bite force and activity with levels of 20–40% (bite dependent) at 30% of the bite cycle and a further increase to 40–60% at 70% of the bite cycle. By contrast, *Codulegaster* shows 30–65% bite-dependent main adductor activity at 30% of the bite cycle and a nearly saturated activity (68–78%) at 70% of the bite cycle. Finally, *Onychogomphus* shows lower activity levels of 12–28% at the beginning of the bite cycle (30%) followed by a steep increase in muscle activity to a nearly saturated level at 70% of the bite cycle. *Onychogomphus* shows a different force and activation development compared with the other species. While *Anax*, *Aeshna* and *Codulegaster* show constantly increasing force and activation, *Onychogomphus* bite force increases rapidly and remains nearly stable for the main part of the bite cycle.

3.3. Spatio-temporal muscle activation

Activation patterns of single muscle groups within the main adductor show a geometry-dependent activation of muscle groups in a comparably simple muscle setting as modelled for *Aeshna*/*Sympetrum* (figure 3*a*). Muscle groups which are located more in the middle part show the highest activation levels during the strongest bite and this pattern is stable for weaker bites (electronic supplementary material, figure S2). In the *Anax* muscle setting with a row of median muscle groups (G10–16; figure 3*b*) within the main adductor, the activation levels of median groups are higher for the three dorsally located groups. By contrast, the main muscle groups (G1–9; figure 3*b*) show more activation in the ventral area of the muscle. In total, 38% of the muscle groups in the *Anax* setting show activation levels below 20%. When two medially located muscle groups are present, as is the case in *Cordulegaster*, activation levels of the medial-most subgroups (G1 – 3 + 5; figure 3*c*) are distinctly lower than those of the other more laterally located subgroups (G4 + 6 – 10). Again, as in *Anax*, the ventral main muscle groups (G17–19) show more activity than the dorsal ones; in total, 53% of all muscle groups show activity levels below 20%. In the spatially most complicated *Onychogomphus* muscle setting 27% of the subgroups show an activity below 20%. Activation patterns for the more medially located muscle subgroups (G1–13; figure 3*d*) are higher than those for the more lateral main muscle groups and there is also a generally higher activity of the dorsal compared with the ventral groups irrespective of their medial or lateral location.

4. Discussion

4.1. Dragonfly bite characteristics

Our results show a trend towards a family-related bite characteristic; however, absolute bite forces are not related to size in our sample. *Onychogomphus*, a medium-sized dragonfly, shows a bite force which is higher than the bite force of *Cordulegaster*, one of the largest dragonflies in Europe (figure 1*b*,

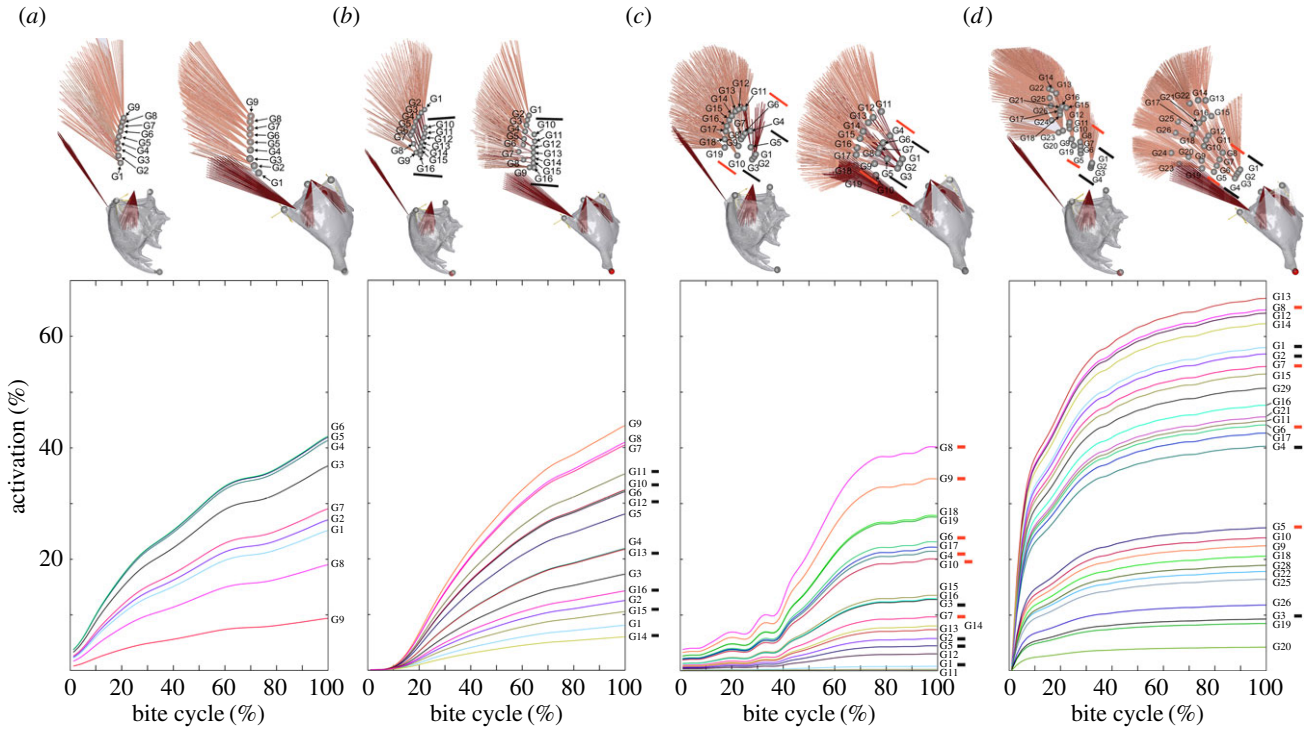

Figure 3. Spatial muscle activation for the main mandibular adductor. Mean activation for each muscle subgroup is shown for the strongest bite measured in each species. (*a*) *Aeshna/Sympetrum*, (*b*) *Anax imperator*, (*c*) *Cordulegaster bidentata*, (*d*) *Onychogomphus forcipatus*. The upper row shows both frontal and lateral views of the muscle groups to faciliate correlation with the graphs, where muscle groups are indicated on the right side, respectively. Black and orange lines in the three-dimensional models correspond to black and orange lines used to highlight medial muscle subgroups in the graphs. For a full overview of activation patterns for several bites and each muscle group within M. craniomandibularis internus please refer to the electronic supplementary material, figure S2. All models are normalized for size.

table 1). Studies of vertebrates showed a strong correlation of size with absolute bite force [51]. As each species was stimulated in the same way and due to the high number of bites recorded, we hypothesize that the higher quantity of subapical muscle groups in *Onychogomphus* compared with the other species allowed for the execution of higher bite forces because this leads to a relatively wider attachment area and an enlarged cross-sectional area at the backside of the head. Indeed, the relative attachment area with respect to specimen size is higher for *Onychogomphus* than for *Cordulegaster* (table 1).

Overall, bite forces are in the range of bite forces measured for other insects [40,52,53]. Taking into account the measured attachment areas, muscle stress in our sample ranged from approximately 21 to 43 N cm^{-2} for the strongest respective bite. Large variations in muscle stress (13–100 N cm^{-2}) have been frequently reported for arthropods including insects depending on the function and geometric relations of muscles [40,53–56].

The mean MA is 0.4 $\pm$ 0.01 and thus is very uniform among the investigated species, which reflects their similar food spectrum. The similar mandibular muscle lever system ratios also means that, despite differing muscle geometries, dragonflies transmit the same percentage of muscle force to the food item.

4.2. Dragonfly muscle activities

Our muscle models are all size corrected; thus, the observed activity differences are only dependent on the spatial composition of the respective muscle and the bite force input. The activity characteristics of the subapical muscle groups only partly fulfilled our expectations. As could be expected, the mandibular adductor with the largest mass (M. craniomandibularis internus, 0md1) showed the highest activity in all species. Additionally, muscle activities (figure 2) show distinct patterns, probably related to the systematic relationships of the species. For example, *Aeshna* and *Anax* are both members of the Aeshnidae, a dragonfly family presumed to represent an early split within dragonflies [57,58], and they both showed largely similar activity time series. However, the subapical muscle groups showed only a distinctly higher activity in *Onychogomphus*, whereas in *Anax* and *Cordulegaster* subapical muscle groups did not show such a distinct pattern (figure 3*b*,*c*). This is also reflected in the significant correlation of the muscle–tendon insertion angle with activation (table 2). It appears that the insertion angles of subapical muscles lead to a higher activation, which might be a result of the suboptimal force transmission at higher angles, an effect frequently reported for human muscle architecture [16,59,60]. Placing more contractile material within a given space at the cost of suboptimal force transmission seems to be overall advantageous in a morphological setting as seen in *Onychogomphus*, whereas this is not the case for the other species with subapical muscle groups.

Bite duration was also highest in *Onychogomphus*. This, together with the conspicuous activity pattern, indicates that the shorter subapical muscles might support a fast development of force which can be preserved on a high level for more than twice as long, as in *Aeshna* and *Anax* (table 1). This ability to act fast and with high duration might be advantageous for medium-sized dragonflies such as *Onychogomphus* in hunting or fighting with larger opponents of different species, as was frequently observed [9].

The occurrence of subapical muscle groups, however, does not seem to be a general evolutionary trend within dragonflies. In Libellulidae, a family consistently recovered as a derived group [57,58,61,62], additional medial muscle groups are very small or even absent [7], consequently also leading

to a lower bite force [10]. It remains to be tested on a larger sample of dragonflies which factors are mainly influencing the evolution of the mandibular muscle system.

Given the sometimes low activity level of single muscle groups (figure 3), it also has to be kept in mind that the theoretical bite forces of species investigated here could be higher. Predictions of bite forces based on musculoskeletal modelling found good agreement with *in vivo* data for a range of vertebrate species [24–26,29,30] so we are confident that the muscle activity levels in our samples are a realistic estimate of the *in vivo* situation. We hypothesize that the attachment at the comparably thin head capsule (figure 1*f*,*g*) might influence absolute muscle output, which leads to the low activity of some muscle groups. Our inverse dynamic data based on the measured bite forces suggest that the theoretical bite force in dragonflies might be distinctly higher in some species such as *Cordulegaster* and *Onychogomphus* but is probably constrained by the head capsule stability.

4.3. Model specifications and model limitations

We investigated the influence of spatial composition of muscle groups in four dragonfly muscle set-ups. These set-ups can be distinguished by the complexity of the main adductor muscle composition. Although musculoskeletal modelling is a technique which has been validated for several groups of animals [24,25,27], a modelling approach for muscles inevitably leads to certain simplifications in muscle representation compared with *in vivo* data. While the origin and insertion points of single fibres are as accurate as the µCT data (3.2–7.9 µm pixel^{-1} in our case, depending on the dataset), other simplifications concern the muscle fibre quantity and the differentiation of muscle subgroups. Muscle fibre quantity has been modelled to our best ability according to the µCT data, but it has to be pointed out that the exact quantity of muscle fibres is likely to be different *in vivo*. Therefore, we do not discuss results concerning forces in single muscle fibres here (such as initial single fibre forces), as these are likely to be biased. Rather, we stick to the overall force production of the muscle, i.e. the muscle stress derived from the PCSA, as the PCSA was measured based on the µCT data. Values for the cross-sectional area are in line with another study focused on a roughly similarly sized insect [52].

We designated muscle groups according to their distinct locations within the muscle, in order to derive information about spatio-temporal muscle subgroup activities. Functional muscle groups *in vivo* are likely to be different and depend on factors such as innervation and neuronal activation patterns during the bite cycle [63]. Muscle subgroup activity patterns as a whole (electronic supplementary material, figure S2), nevertheless, provide an indication about the spatio-temporal muscle fibre activity in the whole muscle. A third topic concerns the movement of the tendon. To model this movement accurately, time-resolved three-dimensional *in vivo* data of tendon movement would be necessary; however, currently only two-dimensional cineradiography at the micrometre scale is available [64]. We, therefore, modelled the tendon movement as a movement to the centre of the muscle insertions at the head capsule. Given the non-significance of the tendon–muscle length ratio with activation (table 2), the modelling of a stiff tendon seems to have no influence on activation patterns of single muscle groups. Previous studies have shown that the tendon of the large mandibular adductor muscle is a complex structure with high variation across the insect orders [2]. It has to be pointed out that some authors use the term 'apodeme' for this structure [65–67], which would imply that the structure is rather sclerotized and stiff, while other authors use the term 'tendon' [4,6,52,68]. Our CT data show that the mandibular 'tendon' has different grey values according to the distance from the mandibular insertion (figure 1*d*–*g*). The highest grey values are found near the mandible, which implies that the density of the material is as high as the density of the stiff mandibles. Towards the muscle insertions, grey values are lower, but are still higher than the surrounding musculature. It can thus be expected that material properties of this structure vary with the distance from the mandible. Clearly, more data are needed to model the 'tendon' material properties for this and other insect muscles with more accuracy.

Data accessibility. The datasets supporting this article have been uploaded as part of the electronic supplementary material.

Authors' contributions. A.B., S.D. and W.P. designed the study. S.D. programmed the AnyBody model, A.B. did the SR-µCT experiments and the segmentation and worked out the analysis pipeline together with S.D. S.D., J.F. and A.B. did the force measurements. A.B. and S.D. wrote the paper; all authors read, corrected and approved the final version of the manuscript.

Competing interests. The authors declare that they have no competing interests.

Funding. Financial support from the Deutsches Elektronen-Synchrotron (DESY: I-20140099) and the PSI (20150464) to perform synchrotron experiments is gratefully acknowledged. A.B. was financed by a research fellowship from the Deutsche Forschungsgemeinschaft (DFG: BL 1355/1-1). S.D. received funding from a graduate fellowship of the German Sports University (DSHS).

Acknowledgements. We thank the Kistler Instrumente AG, namely Christof Sonderegger, for kindly providing the force sensor. We furthermore thank Jürgen Geiermann, who designed and constructed the fixation device. Susanne Duengelhoef, Björn M. von Reumont and Karen Meusemann are thanked for assistance during the SR-µCT experiments. Felix Beckmann, Fabian Wilde (both HZG/DESY), Marco Stampanoni, Rajmund Mokso and Peter Modregger (all PSI) provided excellent support at the synchrotron facilities. The useful discussions with Bernhard Misof and Benjamin Wipfler during the preparation of the manuscript are gratefully acknowledged.

References

1. Grimaldi D, Engel MS. 2005 *Evolution of the insects*. Cambridge, UK: Cambridge University Press.
2. Beutel RG, Friedrich F, Ge SQ, Yang XK. 2014 *Insect morphology and phylogeny*. Berlin, Germany: De Gruyter.
3. Snodgrass RE. 1935 *Principles of insect morphology*. Ithaca, NY: Cornell University Press.
4. Friedemann K, Wipfler B, Bradler S, Beutel RG. 2012 On the head morphology of *Phyllium* and the phylogenetic relationships of Phasmatodea (Insecta). *Acta Zool.* **93**, 184–199. (doi:10.1111/j.1463-6395.2010.00497.x)
5. Friedrich F, Beutel RG. 2010 Goodbye Halteria? The thoracic morphology of Endopterygota (Insecta) and its phylogenetic implications. *Cladistics* **26**, 579–612. (doi:10.1111/j.1096-0031.2010.00305.x)
6. Wipfler B, Machida R, Müller B, Beutel RG. 2011 On the head morphology of Grylloblattodea (Insecta) and the systematic position of the order, with a new nomenclature for the head muscles of

Dicondylia. *Syst. Entomol.* **36**, 241–266. (doi:10.1111/j.1365-3113.2010.00556.x)

7. Blanke A, Greve C, Mokso R, Beckmann F, Misof B. 2013 An updated phylogeny of Anisoptera including formal convergence analysis of morphological characters. *Syst. Entomol.* **38**, 474–490. (doi:10.1111/syen.12012)
8. Staniczek AH. 2000 The mandible of silverfish (Insecta: Zygentoma) and mayflies (Ephemeroptera): its morphology and phylogenetic significance. *Zool. Anz.* **239**, 147–178.
9. Corbet PS. 1999 *Dragonflies: behaviour and ecology of Odonata*. Ithaca, NY: Comstock Publishing Associates.
10. David S, Funken J, Potthast W, Blanke A. 2016 Musculoskeletal modeling of the dragonfly mandible system as an aid to understanding the role of single muscles in an evolutionary context. *J. Exp. Biol.* (doi:10.1242/jeb.132399)
11. Asahina S. 1954 *Morphological study of a relic dragonfly Epiophlebia superstes Selys* (*Odonata, Anisozygoptera*). Tokyo, Japan: Japan Society for the Promotion of Science.
12. Blanke A, Wipfler B, Letsch H, Koch M, Beckmann F, Beutel R, Misof B. 2012 Revival of Palaeoptera—head characters support a monophyletic origin of Odonata and Ephemeroptera (Insecta). *Cladistics* **28**, 560–581. (doi:10.1111/j.1096-0031.2012.00405.x)
13. Short JRT. 1955 The morphology of the head of *Aeshna cyanea* (müller) (Odonata: Anisoptera). *Trans. R. Entomol. Soc. Lond.* **106**, 197–211. (doi:10.1111/j.1365-2311.1955.tb01267.x)
14. Blanke A, Beckmann F, Misof B. 2013 The head anatomy of *Epiophlebia superstes* (Odonata: Epiophlebiidae). *Org. Divers. Evol.* **13**, 55–66. (doi:10.1007/s13127-012-0097-z)
15. Gans C. 1982 Fiber architecture and muscle function. *Exerc. Sport Sci. Rev.* **10**, 160–207. (doi:10.1249/00003677-198201000-00006)
16. Alexander RM, Vernon A. 1975 The dimensions of knee and ankle muscles and the forces they exert. *J. Hum. Mov. Stud.* **1**, 115–123.
17. Muhl ZF. 1982 Active length-tension relation and the effect of muscle pinnation on fiber lengthening. *J. Morphol.* **173**, 285–292. (doi:10.1002/jmor.1051730305)
18. Matsuda R. 1965 Morphology and evolution of the insect head. *Mem. Am. Entomol. Inst.* **1**, 1–334.
19. Pandy MG. 2001 Computer modeling and simulation of human movement. *Annu. Rev. Biomed. Eng.* **3**, 245–273. (doi:10.1146/annurev.bioeng.3.1.245)
20. Johnson WL, Jindrich DL, Roy RR, Edgerton VR. 2008 A three-dimensional model of the rat hindlimb: musculoskeletal geometry and muscle moment arms. *J. Biomech.* **41**, 610–619. (doi:10.1016/j.jbiomech.2007.10.004)
21. Johnson WL, Jindrich DL, Zhong H, Roy RR, Edgerton VR. 2011 Application of a rat hindlimb model: a prediction of force spaces reachable through stimulation of nerve fascicles. *IEEE Trans. Biomed. Eng.* **58**, 3328–3338. (doi:10.1109/TBME.2011.2106784)
22. O'Neill MC, Lee L-F, Larson SG, Demes B, Stern JT, Umberger BR. 2013 A three-dimensional musculoskeletal model of the chimpanzee (*Pan troglodytes*) pelvis and hind limb. *J. Exp. Biol.* **216**, 3709–3723. (doi:10.1242/jeb.079665)
23. Watson PJ, Gröning F, Curtis N, Fitton LC, Herrel A, McCormack SW, Fagan MJ. 2014 Masticatory biomechanics in the rabbit: a multi-body dynamics analysis. *J. R. Soc. Interface* **11**, 20140564. (doi:10.1098/rsif.2014.0564)
24. Gröning F, Jones MEH, Curtis N, Herrel A, O'Higgins P, Evans SE, Fagan MJ. 2013 The importance of accurate muscle modelling for biomechanical analyses: a case study with a lizard skull. *J. R. Soc. Interface* **10**, 20130216. (doi:10.1098/rsif.2013.0216)
25. Curtis N, Jones MEH, Lappin AK, O'Higgins P, Evans SE, Fagan MJ. 2010 Comparison between *in vivo* and theoretical bite performance: using multi-body modelling to predict muscle and bite forces in a reptile skull. *J. Biomech.* **43**, 2804–2809. (doi:10.1016/j.jbiomech.2010.05.037)
26. Curtis N, Jones MEH, Evans SE, Shi J, O'Higgins P, Fagan MJ. 2010 Predicting muscle activation patterns from motion and anatomy: modelling the skull of Sphenodon (Diapsida: Rhynchocephalia). *J. R. Soc. Interface.* **7**, 153–160. (doi:10.1098/rsif.2009.0139)
27. Shi J, Curtis N, Fitton LC, O'Higgins P, Fagan MJ. 2012 Developing a musculoskeletal model of the primate skull: predicting muscle activations, bite force, and joint reaction forces using multibody dynamics analysis and advanced optimisation methods. *J. Theor. Biol.* **310**, 21–30. (doi:10.1016/j.jtbi.2012.06.006)
28. Damsgaard M, Rasmussen J, Christensen ST, Surma E, de Zee M. 2006 Analysis of musculoskeletal systems in the AnyBody Modeling System. *Simul. Model. Pract. Theory* **14**, 1100–1111. (doi:10.1016/j.simpat.2006.09.001)
29. Langenbach G, Zhang F, Herring S, Hannam A. 2002 Modelling the masticatory biomechanics of a pig. *J. Anat.* **201**, 383–393. (doi:10.1046/j.0021-8782.2002.00108.x)
30. Sellers WI, Crompton RH. 2004 Using sensitivity analysis to validate the predictions of a biomechanical model of bite forces. *Ann. Anat. Anat. Anz.* **186**, 89–95. (doi:10.1016/S0940-9602(04)80132-8)
31. Beckmann F, Herzen J, Haibel A, Müller B, Schreyer A. 2008 High density resolution in synchrotron-radiation-based attenuation-contrast microtomography. *Proc. SPIE* **7078**, 70781D–70781D-13. (doi:10.1117/12.794617)
32. Stampanoni M, Marone F, Modregger P, Pinzer B, Thüring T, Vila-Comamala J, David C, Mokso R. 2010 Tomographic hard X-ray phase contrast micro- and nano- imaging at TOMCAT. *AIP Conf. Proc.* **1266**, 13–17. (doi:10.1063/1.3478189)
33. Yushkevich PA, Piven J, Hazlett HC, Smith RG, Ho S, Gee JC, Gerig G. 2006 User-guided 3D active contour segmentation of anatomical structures: significantly improved efficiency and reliability. *NeuroImage* **31**, 1116–1128. (doi:10.1016/j.neuroimage.2006.01.015)
34. Paul J, Gronenberg W. 1999 Optimizing force and velocity: mandible muscle fibre attachments in ants. *J. Exp. Biol.* **202**, 797–808.
35. Paul J. 2001 Mandible movements in ants. *Comp. Biochem. Physiol. A. Mol. Integr. Physiol.* **131**, 7–20. (doi:10.1016/S1095-6433(01)00458-5)
36. Kubo K, Kawakami Y, Fukunaga T. 1999 Influence of elastic properties of tendon structures on jump performance in humans. *J. Appl. Physiol. 1985* **87**, 2090–2096.
37. Duprey S, Savonnet L, Black N, Wang X. 2015 Muscle force prediction: can we rely on musculoskeletal model estimations? A case study on push force exertions with the upper limb. *Comput. Methods Biomech. Biomed. Eng.* **18**(Suppl 1), 1934–1935. (doi:10.1080/10255842.2015.1069575)
38. Zajac FE. 1989 Muscle and tendon: properties, models, scaling, and application to biomechanics and motor control. *Crit. Rev. Biomed. Eng.* **17**, 359–411.
39. Goyens J, Dirckx J, Aerts P. 2015 Costly sexual dimorphism in *Cyclommatus metallifer* stag beetles. *Funct. Ecol.* **29**, 35–43. (doi:10.1111/1365-2435.12294)
40. Goyens J, Dirckx J, Dierick M, Hoorebeke LV, Aerts P. 2014 Biomechanical determinants of bite force dimorphism in *Cyclommatus metallifer* stag beetles. *J. Exp. Biol.* **217**, 1065–1071. (doi:10.1242/jeb.091744)
41. Goyens J, Soons J, Aerts P, Dirckx J. 2014 Finite-element modelling reveals force modulation of jaw adductors in stag beetles. *J. R. Soc. Interface* **11**, 20140908. (doi:10.1098/rsif.2014.0908)
42. Pearson DL. 1988 Biology of tiger beetles. *Annu. Rev. Entomol.* **33**, 123–147. (doi:10.1146/annurev.en.33.010188.001011)
43. Crowninshield RD, Brand RA. 1981 A physiologically based criterion of muscle force prediction in locomotion. *J. Biomech.* **14**, 793–801. (doi:10.1016/0021-9290(81)90035-X)
44. Heintz S, Gutierrez-Farewik EM. 2007 Static optimization of muscle forces during gait in comparison to EMG-to-force processing approach. *Gait Posture* **26**, 279–288. (doi:10.1016/j.gaitpost.2006.09.074)
45. Rasmussen J, Damsgaard M, Voigt M. 2001 Muscle recruitment by the min/max criterion—a comparative numerical study. *J. Biomech.* **34**, 409–415. (doi:10.1016/S0021-9290(00)00191-3)
46. Wang W, Crompton RH, Carey TS, Günther MM, Li Y, Savage R, Sellers WI. 2004 Comparison of inverse-dynamics musculo-skeletal models of AL 288-1 *Australopithecus afarensis* and KNM-WT 15000 *Homo ergaster* to modern humans, with implications for the evolution of bipedalism. *J. Hum. Evol.* **47**, 453–478. (doi:10.1016/j.jhevol.2004.08.007)
47. Westneat MW. 1995 Feeding, function, and phylogeny: analysis of historical biomechanics in labrid fishes using comparative methods. *Syst. Biol.* **44**, 361–383. (doi:10.1093/sysbio/44.3.361)
48. Anderson PSL, Friedman M, Brazeau MD, Rayfield EJ. 2011 Initial radiation of jaws demonstrated

stability despite faunal and environmental change. *Nature* **476**, 206–209. (doi:10.1038/nature10207)
49. Hulsey CD, Wainwright PC. 2002 Projecting mechanics into morphospace: disparity in the feeding system of labrid fishes. *Proc. R. Soc. Lond. B* **269**, 317–326. (doi:10.1098/rspb.2001.1874)
50. Anderson PSL. 2009 Biomechanics, functional patterns, and disparity in Late Devonian arthrodires. *Paleobiology* **35**, 321–342. (doi:10.1666/0094-8373-35.3.321)
51. Dutel H, Herbin M, Clément G, Herrel A. 2015 Bite force in the extant coelacanth *Latimeria*: the role of the intracranial joint and the basicranial muscle. *Curr. Biol.* **25**, 1228–1233. (doi:10.1016/j.cub.2015.02.076)
52. Weihmann T, Reinhardt L, Weißing K, Siebert T, Wipfler B. 2015 Fast and powerful: biomechanics and bite forces of the mandibles in the American cockroach *Periplaneta americana*. *PLoS ONE* **10**, e0141226. (doi:10.1371/journal.pone.0141226)
53. Wheater CP, Evans MEG. 1989 The mandibular forces and pressures of some predacious Coleoptera. *J. Insect Physiol*. **35**, 815–820. (doi:10.1016/0022-1910(89)90096-6)
54. Full R, Ahn A. 1995 Static forces and moments generated in the insect leg: comparison of a three-dimensional musculo-skeletal computer model with experimental measurements. *J. Exp. Biol*. **198**, 1285–1298.
55. Meijden A van der, Langer F, Boistel R, Vagovic P, Heethoff M. 2012 Functional morphology and bite performance of raptorial chelicerae of camel spiders (Solifugae). *J. Exp. Biol*. **215**, 3411–3418. (doi:10.1242/jeb.072926)
56. Taylor GM. 2000 Maximum force production: why are crabs so strong? *Proc. R. Soc. Lond. B* **267**, 1475–1480. (doi:10.1098/rspb.2000.1167)
57. Carle FL, Kjer KM, May ML. 2015 A molecular phylogeny and classification of Anisoptera (Odonata). *Arthropod. Syst. Phylogeny* **73**, 281–301.
58. Fleck G, Ullrich B, Brenk M, Wallnisch C, Orland M, Bleidissel S, Misof B. 2008 A phylogeny of anisopterous dragonflies (Insecta, Odonata) using mtRNA genes and mixed nucleotide/doublet models. *J. Zool. Syst. Evol. Res*. **46**, 310–322. (doi:10.1111/j.1439-0469.2008.00474.x)
59. Rutherford OM, Jones DA. 1992 Measurement of fibre pennation using ultrasound in the human quadriceps *in vivo*. *Eur. J. Appl. Physiol*. **65**, 433–437. (doi:10.1007/BF00243510)
60. Maganaris CN, Baltzopoulos V, Sargeant AJ. 1998 *In vivo* measurements of the triceps surae complex architecture in man: implications for muscle function. *J. Physiol*. **512**(pt 2), 603–614. (doi:10.1111/j.1469-7793.1998.603be.x)
61. Bybee SM, Ogden TH, Branham MA, Whiting MF. 2008 Molecules, morphology and fossils: a comprehensive approach to odonate phylogeny and the evolution of the odonate wing. *Cladistics* **24**, 477–514. (doi:10.1111/j.1096-0031.2007.00191.x)
62. Rehn AC. 2003 Phylogenetic analysis of higher-level relationships of Odonata. *Syst. Entomol*. **28**, 181–240. (doi:10.1046/j.1365-3113.2003.00210.x)
63. Toth TI, Schmidt J, Büschges A, Daun-Gruhn S. 2013 A neuro-mechanical model of a single leg joint highlighting the basic physiological role of fast and slow muscle fibres of an insect muscle system. *PLoS ONE* **8**, e78247. (doi:10.1371/journal.pone.0078247)
64. Schmitt C, Rack A, Betz O. 2014 Analyses of the mouthpart kinematics in *Periplaneta americana* (Blattodea, Blattidae) by using Synchrotron-based X-ray cineradiography. *J. Exp. Biol*. **217**, 3095–3107. (doi:10.1242/jeb.092742)
65. Rähle W. 1970 Untersuchungen an Kopf und Prothorax vom *Embia ramburi* Rimsky-Korsakow 1906 (Embioptera: Embiidae). *Zool. Jbr Anat.* **87**, 248–330.
66. Snodgrass RE. 1954 *The dragonfly larva*. Washington, DC: Smithsonian institution.
67. Kadam K. 1961 Studies on the morphology of an Indian earwig, *Labidura riparia*, Pall., var. ineris, Brunner. *J. Zool. Soc. India* **13**, 34–49.
68. Weihmann T, Kleinteich T, Gorb SN, Wipfler B. 2015 Functional morphology of the mandibular apparatus in the cockroach *Periplaneta americana* (Blattodea: Blattidae)—a model species for omnivore insects. *Arthropod. Syst. Phylogeny* **73**, 477–488.